

Formation of C=C and Si–Cl Adstructures by Insertion Reactions of *cis*-Dichloroethylene and Perchloroethylene on Si(100)2×1

X. J. Zhou, Q. Li, and K. T. Leung*

Department of Chemistry, University of Waterloo, Waterloo, Ontario, N2L 3G1, Canada

Received: October 24, 2005

The room-temperature adsorption and thermal evolution of *cis*-dichloroethylene (DCE) and perchloroethylene (PCE) on Si(100)2×1 have been studied by X-ray photoelectron spectroscopy and temperature programmed desorption (TPD) mass spectrometry. Unlike ethylene that is found to adsorb on Si(100)2×1 through a [2+2] cycloaddition reaction, *cis*-DCE and PCE appear to dechlorinate upon adsorption on the 2×1 surface through an insertion reaction preserving the C=C bond. Our C 1s XPS spectra are consistent with the existence of mono- σ -bonded and di- σ bonded dechlorinated adstructures for both *cis*-DCE and PCE. The presence of the XPS C 1s feature at 283.9 eV, characteristic of the ($=C < \begin{smallmatrix} Si \\ Si \end{smallmatrix}$) component, supports the formation of a unique tetra- σ -bonded C₂ dimer (i.e., by full dechlorination) for PCE, which is found to be stable to 800 K. In marked contrast to PCE for which no organic desorption fragments are observed, *m/z* 26 TPD features at 590 and 750 K have been observed for *cis*-DCE. These features could be attributed to the formation of acetylene resulting from Cl β -elimination of 2-chlorovinyl adspecies and to direct desorption of vinylene, respectively. Further annealing the *cis*-DCE and PCE samples to above 800 K produces SiC and/or carbon clusters. The TPD data also show HCl evolution over 810–850 K for both *cis*-DCE and PCE, the latter of which also exhibits an additional SiCl₂ evolution above 850 K. The present work illustrates that the insertion mechanism could be quite common in the surface chemistry of chlorinated ethylenes on the 2×1 surface.

1. Introduction

Organosilicon surface chemistry has been the subject of extensive experimental and theoretical investigations in the past decade. For instance, Hamers et al. demonstrated that ordered monolayers of organic compounds with the appropriate functional groups can be deposited on Si(100) to serve as templates for further attachment of “linker” biomolecules to DNA and other biomolecular systems.^{1,2} This type of biomolecular silicon interface is of great importance to both biotechnology and semiconductor industries, particularly for use as the basic platform for integrating biosensors directly onto a silicon chip. It would therefore be of interest to investigate the growth of ordered and selective functionalized monolayers on such a benchmark surface as Si(100)2×1, to develop better understanding of the underlying mechanisms and potential industrial applications. Understanding the surface interactions and reactions between prototypical organic molecules and silicon is fundamental to the design and ultimate control of the biomolecular silicon interface. Previous studies on saturated hydrocarbon molecules have revealed no adsorption on Si(100)2×1 at room temperature (RT),³ in marked contrast to their unsaturated counterparts. In particular, ethylene and acetylene are found to react with the Si dimers on the 2×1 surface in a cycloaddition mechanism that involves breakage of the weak “ π bond” in the Si dimer while leaving the strong σ bond intact.^{1,4} Although the alternative insertion mechanism (in which a Si substrate atom is inserted into a C–H bond) has been proposed for ethylene and acetylene, more recent studies (with some supported by theoretical calculations) have demonstrated that the σ bond of the Si dimer is hardly perturbed,^{5–8} in good accord with the

cycloaddition mechanism. On the other hand, several studies have provided strong evidence for dissociative adsorption for halogenated saturated^{9,10} and unsaturated hydrocarbons^{11,12} on Si(111)7×7 and Si(100)2×1. These observations are consistent with similar dissociative adsorption found for molecular halogen (F₂, Cl₂, Br₂) on Si(100)2×1.^{13–15} Our recent work has shown that upon adsorption on Si(100)2×1 dibromoethylene (DBE) undergoes Br dissociation involving insertion of a Si dimer atom into the C–Br bond, in effect forming a di- σ bonded vinylene (i.e., ethen-1,2-diyl) bridge.¹² There are two possible mechanisms for the insertion reactions. In the first mechanism, the C=C bond is broken by the formation of a diradical intermediate with the Si dangling bond and subsequently reformed by double dehalogenation, producing the Si–X bonds (where X is the halogen atom). Alternatively, a π -complex (or 3-atom intermediate) is formed with a Si atom of the Si dimer, while the halogen is abstracted by the other Si atom. Furthermore, as observed by Bronikowski and Hamers,⁹ the strongly localized nature of the Si–X bond (where X is Cl or Br) prevents the halogen atom from surface migration to other sites at RT. It is therefore quite plausible to form an ordered monolayer of halogen atoms, with the vinylene group occupying the intervening rows of the Si(100)2×1 surface. Both the cycloaddition and insertion mechanisms can be further exploited to facilitate selective functionalization and to develop templates for building extended molecular structures.

In the present work, we extend our earlier study on DBE to *cis*-dichloroethylene (DCE) on Si(100)2×1 to investigate the effects of different halogens (i.e., Cl vs Br) on the underlying adsorption mechanism (i.e., cycloaddition vs insertion) and on the thermally driven surface chemistry (i.e., etching reaction vs recombinative desorption of hydrogen halide). Our temper-

* Address correspondence to this author. E-mail: tong@uwaterloo.ca.

ature programmed desorption (TPD) data on DBE/Si(100)2×1 have revealed recombinative desorption of HBr with maxima at 830 and 950 K,¹² i.e., without any Si-containing desorbates (etching products). It would therefore be of special interest to determine whether the replacement by the generally more reactive and electronegative Cl atoms as in DCE would lead to additional thermally driven surface reactions, including surface etching. Furthermore, tetrachloroethylene or perchloroethylene (PCE) is also investigated in order to identify the roles of molecular structures and symmetries, particularly those with only Cl ligands, on the initial chemisorption properties and the aforementioned surface processes.

2. Experimental Details

All the experiments were performed in a home-built dual-chamber ultrahigh vacuum (UHV) system with a base pressure better than 1×10^{-10} Torr.¹⁶ The sample preparation chamber was equipped with an ion-sputtering gun for sample cleaning, and four-grid retarding-field optics for both reverse-view low energy electron diffraction (LEED) and Auger electron spectroscopy, while the analysis chamber was used to conduct TPD and X-ray photoelectron spectroscopy (XPS) studies. A 14×7 mm² substrate was cut from a single-side polished p-type B-doped Si(100) wafer (0.4 mm thick) with a resistivity of 0.0080–0.0095 Ω cm. Details of the sample mounting and preparation procedures have been described in our earlier work.¹⁶ The liquid chemicals, *cis*-DCE (97% purity) and PCE (99.9% purity), were purchased from Aldrich and thoroughly degassed by repeated freeze–pump–thaw cycles, prior to exposure to the Si sample by backfilling the preparation chamber to an appropriate pressure (as monitored by an uncalibrated ionization gauge) with a variable precision leak valve. All exposures (in units of Langmuir, 1 L = 1×10^{-6} Torr s) were performed at RT and a saturation coverage was used for all the TPD and XPS experiments unless stated otherwise.

In our TPD experiments, the Si sample was positioned 2 mm from the orifice of the differentially pumped chamber that housed a 1–300 amu quadrupole mass spectrometer (QMS). The desorbates were ionized in the ionizer region of the QMS, and the detected ions were monitored as a function of the sample temperature. A home-built programmable proportional-integral-differential temperature controller was used to provide linear temperature ramping at an adjustable heating rate, typically set at 2 deg/s.¹⁶ The absolute accuracy of our temperature measurement obtained by an uncalibrated type K thermocouple directly attached to the sample was estimated to be ± 20 K.

XPS experiments were performed at RT by using an electron spectrometer consisting of a hemispherical analyzer (of 100 mm mean radius) and a triple-channeltron detector, with a twin-anode X-ray source that provided unmonochromatic Al K α radiation (with a photon energy of 1486.6 eV). XPS spectra were collected with an acceptance angle of $\pm 4^\circ$ at normal emission from the silicon sample, and with a constant pass energy of 50 eV giving an effective energy resolution of 1.4 eV full-width-at-half-maximum (for the Si 2p photopeak). The binding energy scale of the XPS spectra used in the present work has been calibrated to the Si 2p feature of the bulk at 99.3 eV.¹⁷ Spectral fitting and deconvolution based on residual minimization with Gaussian–Lorentzian line shapes were performed by using the CasaXPS software. For temperature-dependent XPS measurements, the sample was flash-annealed to a preselected temperature and quenched to RT before collecting the XPS spectra at RT. To avoid ambiguity in the quantification of the surface Cl content based on the Cl 2p

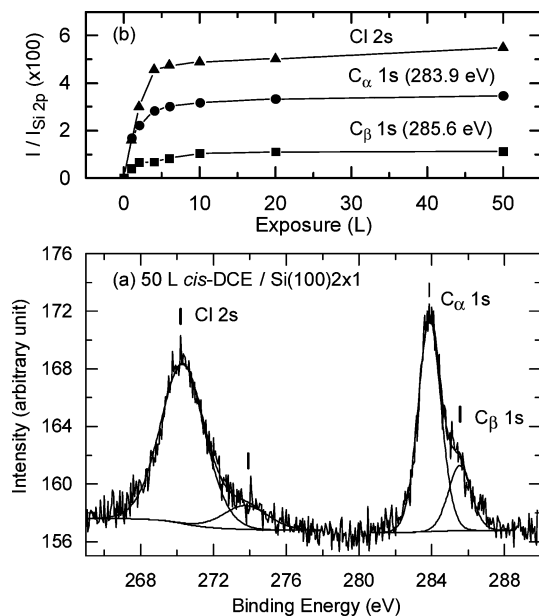


Figure 1. (a) XPS spectra of the Cl 2s and C 1s regions of 50 L of *cis*-dichloroethylene (DCE) exposed to Si(100)2×1 at room temperature. (b) The intensity (I) ratios of the total Cl 2s envelope (\blacktriangle) and C $_{\alpha}$ 1s at 283.9 eV (\bullet) and C $_{\beta}$ 1s at 285.6 eV (\blacksquare), all with respect to the Si 2p feature at 99.3 eV, as a function of exposure.

photopeak near 200 eV (because of the often ill-defined background contribution arising from the nearby Si 2s feature at 151 eV), the Cl 2s photopeak at 270 eV was used instead in all the experiments.

3. Results and Discussion

3.1. Room-Temperature Chemisorption and Thermal Evolution of *cis*-Dichloroethylene. Figure 1a shows a typical XPS spectrum of the C 1s and Cl 2s regions for a 50 L exposure of *cis*-DCE on Si(100)2×1 at RT. An intense and a discernibly weaker C 1s feature at binding energies of 283.9 and 285.6 eV, respectively, could clearly be identified. Using synchrotron radiation at 391 eV photon energy, Fink et al.¹⁸ also observed two well-defined C 1s photopeaks at similar binding energies (283.8 and 285.4 eV) for 1,2-DCE adsorbed on Si(100)2×1 at 80–100 K (but with reverse relative intensities for the two peaks). To identify the plausible adsorption geometries and hence to attribute them to the appropriate XPS features, we performed ab initio density functional calculations using Gaussian 03,¹⁹ with hybrid functionals consisting of Becke's 3-parameter nonlocal exchange functional and the correlation functional of Lee–Yang–Parr (the so-called B3LYP method in Gaussian 03).²⁰ A Si₁₅H₁₆ cluster was used to approximate the Si(100)2×1 surface with two Si dimers, and two *cis*-DCE molecules were used in order to better expose any adsorbate–adsorbate interaction and subsequent effects on the adsorption process. The 6-31G(d) and 6-311G(d) basis sets have been used and found to give qualitatively similar adsorption geometries. Figure 2 shows the corresponding adsorption geometries obtained with the 6-31G(d) basis set for two local energy minima. In particular, the first local minimum corresponds to a di- σ bonded vinylene adstructure with total dechlorination by in effect insertion of two Si surface atoms into the C–Cl bonds (Figure 2a), which gives rise to one type of C local environment (i.e., the ipso carbon as in $=C_{\alpha} < \frac{H}{Si}$). The corresponding energy change ΔE , with the zero-point vibrational energy correction, for the formation of a vinylene adspecies and two dissociated Cl atoms on the surface of the Si₁₅H₁₆ cluster is calculated to

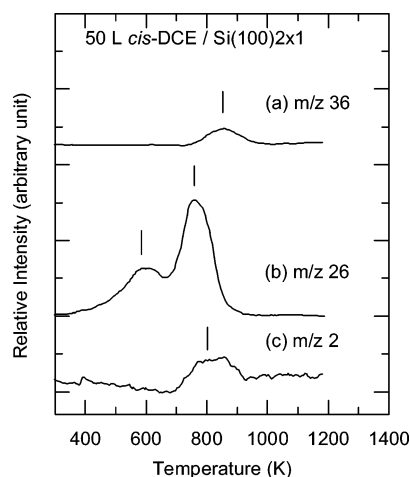
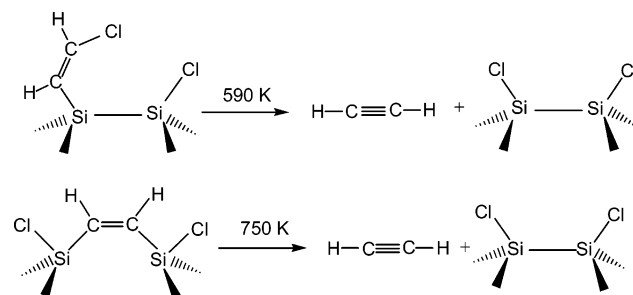


Figure 3. Temperature programmed desorption profiles of (a) m/z 36 (HCl^+), (b) m/z 26 (C_2H_2^+), and (c) m/z 2 (H_2^+) for 50 L of *cis*-dichloroethylene exposed to $\text{Si}(100)2\times 1$ at room temperature.

The XPS spectra of the Cl 2s and C 1s regions for *cis*-DCE on $\text{Si}(100)2\times 1$ have also been measured as a function of exposure at RT (not shown). No changes in the binding energies for the C_α 1s, C_β 1s, and Cl 2s features with increasing exposure have been observed. The corresponding relative intensity ratios of the C_α 1s, C_β 1s, and Cl 2s features, all with respect to the Si 2p feature at 99.3 eV, are shown in Figure 1b. These profiles indicate that saturation coverage is reached at 6 L. Given the proportional increase in the relative intensities of C_α and C_β with increasing exposure, there is no obvious preference for adsorption involving di- σ or mono- σ bonding. Furthermore, the effective constant intensity ratio between the overall C 1s envelope (i.e., C_α 1s + C_β 1s) and the Cl 2s feature is found to be ~ 1.2 . This intensity ratio corresponds to the ratio of relative concentration of C on the surface to that of Cl on the surface, after appropriately taking into account the semiempirical Wagner atomic sensitivity factors.²⁴ The effective unity C/Cl ratio suggests that no differential desorption of C- or Cl-containing adspecies occurs over the entire exposure range at RT. All of the fragments as a result of dissociative adsorption for *cis*-DCE on $\text{Si}(100)2\times 1$ at RT therefore remain adsorbed on the surface, which is similar to that found for methyl chloride²⁵ and methyl iodide.¹⁰ The strong adsorption at RT indicates strong interaction between *cis*-DCE and the $\text{Si}(100)2\times 1$ surface, which is consistent with the large magnitudes of the ΔE values obtained in the above calculation.

Figure 3 shows the TPD profiles of selected ions for a 50 L (saturation) exposure of *cis*-DCE on $\text{Si}(100)2\times 1$. Following our earlier work on DBE,¹² we focus on the thermal evolution of similar ions, particularly the parent ions of HCl, C_2H_2 , and H_2 with m/z of 36, 26, and 2, respectively. Other fragments including those with m/z of 96 ($\text{C}_2\text{H}_2\text{Cl}_2^+$ or the parent ion), 94 (C_2Cl_2^+), and 61 ($\text{C}_2\text{H}_2\text{Cl}^+$) have also been monitored but no desorption features were found. The absence of m/z 96 therefore supports dechlorination of *cis*-DCE upon adsorption, as inferred from our XPS data (Figure 1). Evidently, recombinative desorption of hydrogen halide from the dissociated halogen atom and surface H atom can be observed for both DBE¹² and DCE on $\text{Si}(100)2\times 1$. In particular, a broad TPD feature of m/z 36 (HCl^+) extending over 780–930 K with desorption maximum at 850 K (Figure 3a) is found to occur at a lower temperature region than the m/z 80 (HBr^+) feature at 800–1100 K for DBE (Figure 3 in ref 12). HCl desorption was further confirmed by the desorption intensity of ion at m/z 35 proportional to m/z 36 at the same desorption temperature

SCHEME 1^a



^a It should be noted that even though dissociated Cl atoms are shown to occupy the same Si dimer, these Cl atoms could also be located at different Si dimers.

maximum. Like HBr desorption,¹² the m/z 36 feature can be attributed to multiple desorption channels involving, e.g., recombination of the dissociated Cl atoms with resident surface H atoms and H atoms abstracted from the adsorbed hydrocarbons (such as ethyl species). The occurrence of the HCl desorption at a lower temperature region than HBr desorption¹² suggests a greater surface mobility for the Cl atoms than the Br atoms. However, the Si-Cl bond (with bond strength $\Delta H_B = 109$ kcal/mol) is thermodynamically more stable than the Si-Br bond (with $\Delta H_B = 82$ kcal/mol),²¹ which therefore indicates that kinetic effects play a more important role in the recombinative desorption of these halogen halides on $\text{Si}(100)$. The presence of surface H atoms likely in the form of Si monohydrides for the adsorption of both *cis*-DCE (Figure 3c) and DBE on $\text{Si}(100)2\times 1$ ¹² is also confirmed by the m/z 2 desorption feature at 800 K, which corresponds to recombinative desorption of H_2 from Si monohydrides. In the case of m/z 26 desorption, two strong TPD features are observed in Figure 3b. As illustrated schematically in Scheme 1, the two m/z 26 desorption features likely correspond to C_2H_2 desorption from mono- σ bonded chlorovinyl adspecies upon Cl elimination near 590 K and from di- σ bonded vinylene adspecies upon breakage of two Si-C bonds near 750 K. The higher desorption maximum of the m/z 26 feature at 750 K (Figure 3b) is consistent with the larger energy required for breaking two Si-C bonds. This higher temperature TPD feature is therefore similar to that at 770 K found for DBE.¹²

To further investigate the adspecies remaining on the surface during the thermal desorption process, XPS spectra of the Cl 2s and C 1s regions for a 50 L RT exposure of *cis*-DCE on $\text{Si}(100)2\times 1$ were collected at RT after sequentially flash-annealing to preselected temperatures, and are shown in Figure 4. The three well-defined features corresponding to Cl 2s at 270.3 eV, C_α 1s at 283.9 eV, and C_β 1s at 285.6 eV (as depicted previously in Figure 1a) remain essentially unchanged upon annealing the sample to 620 K (Figure 4c). An additional C 1s feature at 283.0 eV corresponding to SiC is seen to emerge above 800 K (Figure 4d). The corresponding thermal evolution of the intensities of these Cl 2s and C 1s features relative to that of Si 2p (at 99.3 eV) is shown in Figure 4g. In accord with our TPD data for m/z 36 (Figure 3a), no significant reduction in the Cl relative concentration, as indicated by the lack of any significant intensity change observed for Cl 2s, is found below 800 K (Figure 4g). Furthermore, the weakening of the C_β 1s peak (at 285.6 eV) above 620 K indicates reduction in the relative surface concentration of the 2-chlorovinyl adspecies. This is again in agreement with the thermal evolution of mono- σ bonded 2-chlorovinyl adspecies (Scheme 1), as represented by the m/z 26 TPD feature near 590 K (Figure 3b). Between 700 and 800 K, the reduction in the residual concentration of the

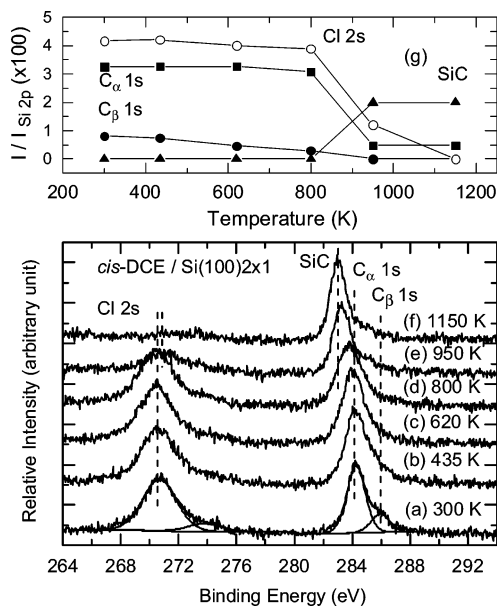


Figure 4. XPS spectra of the Cl 2s and C 1s regions of (a) 50 L of *cis*-dichloroethylene (DCE) exposed to Si(100)2×1 at room temperature and after sequential flash-annealing to (b) 435, (c) 620, (d) 800, (e) 950, and (f) 1150 K. The intensity (*I*) ratios of the total Cl 2s envelope (○) and C_α 1s at 283.9 eV (■), C_β 1s at 285.6 eV (●), and C 1s of SiC at 283.0 eV (▲), all with respect to the Si 2p feature at 99.3 eV, are shown in panel g).

di- σ bonded vinylene adspecies as a result of acetylene (*m/z* 26) desorption (Scheme 1) is consistent with the decrease in the C_α 1s relative intensity (Figure 4d). Above 800 K, the remaining hydrocarbon adspecies are evidently converted to SiC, which gives rise to an increase in the C 1s feature at 283.0 eV and the apparent C 1s band movement to the lower binding energy as shown in Figure 4e. Finally, the Cl 2s feature at 270.3 eV is found to become weakened and shifted to 271.0 eV upon annealing the sample to 950 K (Figure 4e). This higher binding energy of the Cl 2s peak could be attributed to residual Cl atoms attached to C clusters likely nucleated at the SiC or defect sites, which is consistent with the smaller calculated Cl 2s orbital energy for Si–Cl than that for C–Cl adspecies by 0.6 eV, as discussed above. Annealing the sample to 1150 K completely removes the Cl 2s feature (Figure 4f), leaving the SiC feature behind.

3.2. Room-Temperature Chemisorption and Thermal Evolution of Perchloroethylene. Figure 5 compares the XPS spectrum of the C 1s and Cl 2s regions for a 50 L RT exposure of PCE on Si(100)2×1 with that of *cis*-DCE. Three C 1s features at 283.9 (Feature 7), 285.2 (Feature 8), and 287.0 eV (Feature 9) corresponding to different local C environments are clearly evident in Figure 5b. To assign these features, we also performed similar hybrid density functional calculations at the B3LYP/6-31G(d) level (as discussed above), using the double-dimer surface of the Si₁₅H₁₆ cluster to model the Si(100)2×1 surface. To avoid the unrealistic edge distortion in the cluster structure during the geometry optimization, the atoms in the bottom three layers of the Si₁₅H₁₆ cluster were frozen to maintain a reasonable bulk geometry while keeping only the surface layer and the adspecies fully relaxed. Figure 6 illustrates five possible adsorption geometries for PCE on the model double-dimer surface, along with their respective adsorption energies ΔE (with the zero-point vibrational energy corrections). Like *cis*-DCE, the adsorption of PCE on the model surface could also involve single dechlorination with mono- σ bonded trichlorovinyl adspecies (Figure 6a) or double dechlorination with di- σ bonded

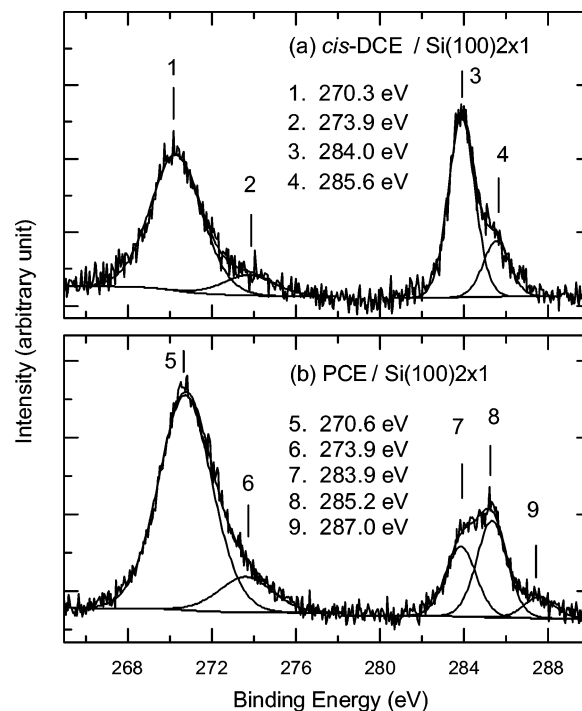


Figure 5. XPS spectra of the Cl 2s and C 1s regions of (a) 50 L of *cis*-dichloroethylene (DCE) and (b) perchloroethylene (PCE) exposed to Si(100)2×1 at room temperature.

adspecies to the Si surface (Figure 6b–d), all with the C=C bond intact. The mono- σ bonded trichlorovinyl adspecies ($\Delta E = -63.3$ kcal/mol) is found to be generally less tightly bonded than the di- σ bonded adstructures ($\Delta E = -77.8$ to -114.1 kcal/mol). In the latter case, we could further distinguish the adsorption of the di- σ bonded species according to the different adsorption arrangements on the surface sites. In particular, the dichlorovinylene (or 1,2-dichloroethenediyl) adspecies di- σ bonded perpendicular to the dimer row in the so-called cross-dimer bridge adstructure with $\Delta E = -77.8$ kcal/mol (Figure 6b) is found to be the least stable of the three di- σ bonded adstructures. The dichlorovinylene adspecies in the in-plane dimer bridge geometry with $\Delta E = -114.1$ kcal/mol (Figure 6c) also appears to be more stable than the di- σ bonded dichlorovinylidene (or 1,1-dichloroethenediyl) adspecies in the out-of-plane dimer bridge geometry with $\Delta E = -97.7$ kcal/mol (Figure 6d). The relative stabilities of the adstructures can be understood in terms of the structural compatibility of the adspecies with respect to the local geometry of the adsorption site of the substrate. In the top layer, the calculated Si–Si separation between two dimers in parallel (3.9 Å) is found to be 0.4 Å longer than that within a dimer (3.5 Å). In addition, full dechlorination of PCE on the model surface could lead to an ethenetetrayl (or C₂ dimer) adspecies tetra- σ bonded to two Si dimers in the so-called X-bridge geometry (Figure 6e). With $\Delta E = -194.5$ kcal/mol, the C₂ dimer X-bridge adstructure appears to be the most stable of all the adsorption structures investigated by us thus far. The negative magnitudes of the adsorption energies obtained for the five adstructures suggest that all five adstructures are thermodynamically feasible. The relative magnitudes of the adsorption energies are found to be consistent with the number of Si–C σ bonds (between the adspecies and the Si substrate). Of the five calculated adstructures shown in Figure 6, we also identify three possible types of local carbon environments: C_a in ($=C_a < \overset{Si}{Si}$), C_b in ($=C_b < \overset{Cl}{Si}$), and C_c in ($=C_c < \overset{Cl}{Cl}$), corresponding to C atoms attached to 0 (2), 1 (1), and 2 (0) chlorine (silicon) atoms,

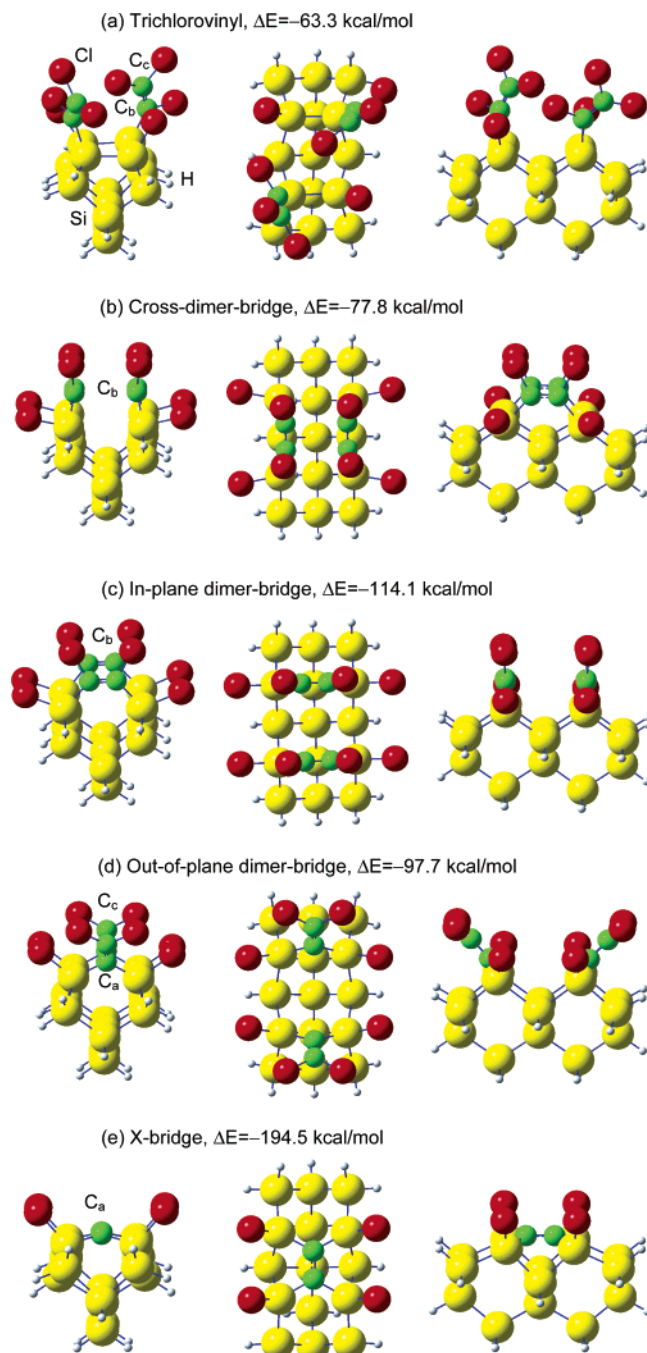


Figure 6. Schematic diagrams of the adsorption geometries and the corresponding adsorption energies, ΔE , for (a) trichlorovinyl adstructure, dichlorovinylene at (b) the cross-dimer-bridge and (c) in-plane dimer-bridge sites, (d) dichlorovinylidene at the out-of-plane dimer-bridge site, and (e) the C_2 dimer at the X-bridge site. These perchloroethylene adstructures are obtained on the model surface of a $Si_{15}H_{16}$ cluster (with all the layers except for the topmost layer frozen) by a density functional calculation at the B3LYP/6-31G(d) level.

respectively. In accord with the electronegativities (Pauling scale) of Si (1.8), C (2.5), and Cl (3.0),²⁶ the ordering of the C 1s binding energies should follow the trend C_a 1s < C_b 1s < C_c 1s. We therefore assign the XPS features at 283.9 (Feature 7), 285.2 (Feature 8), and 287.0 eV (Feature 9) in Figure 5b to C_a 1s, C_b 1s, and C_c 1s, respectively. It should be noted that the present assignments for C 1s at 285.2 and 287.0 eV are consistent with the assignments for similar adspecies observed for PCE on Pd(100) at 291 K by Park et al.²⁷ and on Pt(111) at 90 K by Cassuto et al.²⁸ Furthermore, given the similarities in

the electronegativities of Si (1.8) and H (2.1), the binding energies of C_a 1s (283.9 eV) and C_b 1s (285.2 eV) for PCE (Figure 5b) should therefore be similar to those for C_α 1s in ($=C_\alpha < \overset{H}{Si}$) at 284.0 eV and C_β 1s in ($=C_\beta < \overset{H}{Cl}$) at 285.6 eV (Figure 5a) observed for DCE, respectively (Figure 5a). As comparison, the C 1s in ($=C_\eta < \overset{H}{H}$) is generally found at 284.8,²⁹ and the corresponding ordering of the C 1s binding energies therefore follows the trend C_α 1s < C_η 1s < C_β 1s.

The relative intensity ratio of the C_a 1s (Feature 7) to C_b 1s (Feature 8) to C_c 1s (Feature 9) is found to be approximately 4:5:1 (Figure 5b). The presence of C_c 1s indicates the existence of the di- σ bonded dichlorovinylidene adspecies (Figure 6d) and mono- σ bonded trichlorovinyl adspecies (Figure 6a) as the only two possible adspecies containing a ($=C_c < \overset{Cl}{Cl}$) group. Given that the latter mono- σ trichlorovinyl adspecies is found to be considerably less thermodynamically stable than the di- σ bonded dichlorovinylidene, we expect the relative concentration of dichlorovinylidene to be greater than that of trichlorovinyl adspecies. Furthermore, because the relative population of ($=C_\alpha < \overset{Si}{Si}$) and ($=C_c < \overset{Cl}{Cl}$) in dichlorovinylidene (Figure 6c) should be 1:1, the discernibly extra population of C_a as reflected by the C_a 1s to C_c 1s XPS intensity ratio of 5:1 provides strong evidence for the presence of the novel tetra- σ bonded ethene-tetrayl (or C_2 dimer) adspecies (Figure 6e). The C_2 dimer adspecies in this particular adsorption geometry is novel because not only has such a species never been observed on Si single-crystal surfaces before but also such an adspecies is found to exhibit the lowest ΔE . This adstructure is expected to be “inert” and protected from further surface reactions due to total blockage by the Cl atoms. Moreover, the significant amount of C_b 1s intensity indicates the presence of dichlorovinylene adspecies [with the adstructure likely favoring the more stable in-plane dimer bridge (Figure 6c) than the cross-dimer bridge geometry (Figure 6b)], while the contribution from the mono- σ bonded trichlorovinyl adspecies (Figure 6a) cannot be ruled out.

Figure 5b also shows that the Cl 2s XPS spectrum for a saturation coverage of PCE on $Si(100)2 \times 1$ at RT is similar to that of *cis*-DCE (Figure 5a) and can therefore be given a similar assignment. In particular, the broad photopeak at 270.6 eV (Feature 5) can be attributed to a mixture of Cl–Si and Cl–C bonds (with chemical shifts not discernible in the present experiment), while the shoulder at 273.9 eV (Feature 6) is consistent with the shake-up processes, as discussed above. It is noteworthy that the total intensity ratios of the Cl 2s photopeaks to C 1s photopeaks for PCE/ $Si(100)2 \times 1$ (1.65) and that for *cis*-DCE/ $Si(100)2 \times 1$ (0.86) are in qualitative accord with the relative Cl-to-C concentrations in the respective chlorinated ethylenes. This observation therefore supports our hypothesis that the Cl atoms largely remain on the surface as part of the adsorbed chlorinated ethylene adspecies or as dissociated atoms bonding directly to the Si substrate, upon adsorption of PCE or *cis*-DCE.

Figure 7 shows the TPD profiles of observed desorbates with their corresponding ions including m/z 98 ($SiCl_2^+$), 63 ($SiCl^+$), and 36 (HCl^+) for a 50 L (saturation) exposure of PCE on $Si(100)2 \times 1$ at RT. Evidently, the desorption features for m/z 98 and 63 with desorption maxima at 870 and 900 K, respectively, are similar to each other, which indicates that the desorbed fragment is most likely $SiCl_2$. A similar etching effect has also been observed for PCE on a metal surface, such as Fe(110) with $FeCl_2$ as the etchant product.³⁰ The desorption of $SiCl_2$ could also follow a similar mechanism involving dichloride isomerization on Cl-saturated $Si(100)$ as proposed by Nakayama et al.³¹ The m/z 36 profile for PCE, with a desorption maximum

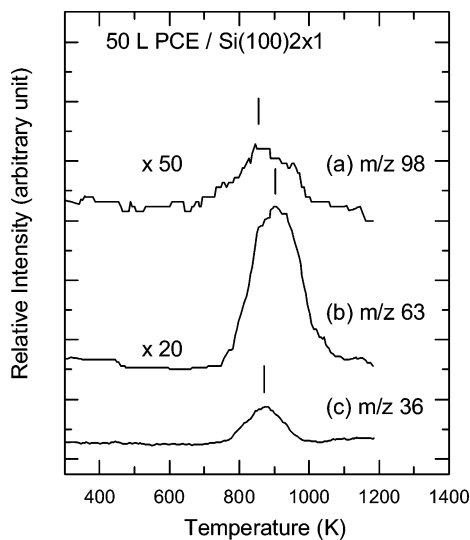


Figure 7. Temperature programmed desorption profiles of (a) m/z 98 (SiCl_2^+), (b) m/z 63 (SiCl^+), and (c) m/z 36 (HCl^+) for 50 L of perchloroethylene (PCE) exposed to $\text{Si}(100)2 \times 1$ at room temperature.

at 870 K, is found to be in good accord with that observed for *cis*-DCE (Figure 3a) previously attributed to desorption of HCl. In the case of PCE, the m/z 36 TPD feature could also be due to recombinative desorption of HCl, from the dissociated Cl atoms originating from the proposed PCE adsorption and H atoms likely due to dissociation of residual water commonly present in UHV chambers. The presence of only a small quantity of H atoms on the surface is clearly supported by the absence of any m/z 2 desorption feature, unlike the *cis*-DCE case for which a discernible m/z 2 feature due to recombinative desorption of H_2 from monohydrides is clearly observed at 800 K (Figure 3a). In contrast to *cis*-DCE (Figure 3), the presence of the SiCl_x ($x = 1$ or 2) etching products for the PCE sample (Figure 7b,c) suggests that the production of SiCl_x would proceed upon near exhaustion of surface H atoms. The abundance of H atoms provided by the *cis*-DCE adsorption facilitates continued recombinative desorption of HCl, therefore preventing the formation of SiCl_x etchant products. Like *cis*-DCE (Figure 3), the TPD profile of the corresponding base mass for PCE (m/z 129, corresponding to C_2Cl_3^+) has also been monitored but no discernible feature was found, suggesting that molecular desorption of PCE (and *cis*-DCE) is not a prominent process on $\text{Si}(100)2 \times 1$. Other fragments including those with m/z of 47 (CCl^+), 82 (CCl_2^+), 94 (C_2Cl_2^+), 117 (CCl_3^+), 133 (SiCl_3^+), 152 (CCL_4^+), 164 (C_2Cl_4^+), and 168 (SiCl_4^+) have also been monitored and their TPD profiles revealed no desorption features.

Figure 8 shows the complementary XPS spectra of the Cl 2s and C 1s regions collected at RT for a 50 L RT exposure of PCE on $\text{Si}(100)2 \times 1$ after sequentially flash-annealing to pre-selected temperatures. The relative intensities of the C 1s and Cl 2s features with respect to the Si 2p peak at 99.3 eV of the substrate have been obtained after appropriate deconvolution by using a curve fitting procedure, and they are shown as a function of annealing temperature in Figure 8g. Upon annealing the sample to 620 K, the relative intensity of the C_c 1s feature at 287.0 eV is nearly completely diminished, while that for the C_b 1s peak at 285.2 eV becomes considerably reduced to a finite residual intensity (Figure 8c). On the other hand, the intensity of the C_a 1s feature at 283.9 eV appears to reach a maximum near the annealing temperature of 620 K (Figure 8c) and becomes reduced upon further annealing to above 800 K. These

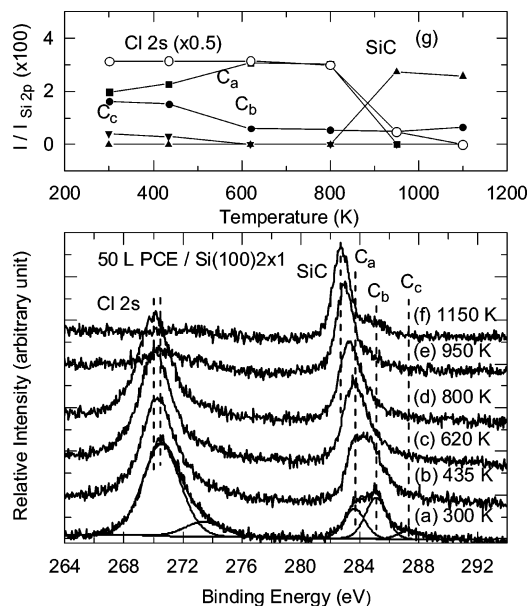


Figure 8. XPS spectra of the Cl 2s and C 1s regions of (a) 50 L of perchloroethylene (PCE) exposed to $\text{Si}(100)2 \times 1$ at room temperature and after sequential flash-annealing to (b) 435, (c) 620, (d) 800, (e) 950, and (f) 1150 K. The intensity (I) ratios of the Cl 2s envelope (\circ) and C_a 1s at 283.9 eV (\blacksquare), C_b 1s at 285.2 eV (\bullet), C_c 1s at 287.0 eV (\blacktriangledown), and C 1s of SiC at 283.0 eV (\blacktriangle), all with respect to Si 2p at 99.3 eV, are shown in panel g.

intensity changes are consistent with the thermal evolution of our proposed adspecies (Figure 6), which undergo continued dechlorination causing the reductions in the relative amounts of the ($=\text{C}_c < \text{Cl}$) component and then the ($=\text{C}_b < \text{Si}$) component. The reductions in these components are correlated with the corresponding increase in the amount of the ($=\text{C}_a < \text{Si}$) component, as shown in our XPS results. It should be noted that the C 1s feature for carbon clusters has been found to be at 285.0 eV, which accounts for the finite intensity of the feature at 285.2 eV upon annealing to above 800 K. A new C 1s feature at 283.0 eV is also found to emerge upon annealing the sample to above 800 K and become the most prominent feature at 1150 K (Figure 8f), in good accord with the formation of SiC above 800 K observed for the *cis*-DCE sample (Figure 4e,f).

In the case of the Cl 2s peak at 270.6 eV, no significant change is observed in the intensity up to the flash-annealing temperature of 800 K (Figure 8d), above which a dramatic reduction is found at 950 K (Figure 8e). In contrast to the Cl 2s feature for *cis*-DCE (Figure 4a–f) that remains stationary with the flash-annealing temperature, the Cl 2s peak maximum for PCE appears to shift slightly to 270.3 eV upon annealing the sample to 435 K (Figure 8b). This apparent shift is in good accord with the onset of the proposed dechlorination, which increases the Si–Cl relative concentration (with Cl 2s at 270.3 eV) at the expense of the C–Cl relative concentration (with Cl 2s at 270.6 eV). Upon annealing the sample to 950 K, not only is the Cl 2s peak intensity greatly reduced, but the peak maximum appears to revert back to 271.0 eV. Like the *cis*-DCE case, this higher binding energy for the Cl 2s peak could be attributed to residual Cl atoms attached to C clusters likely nucleated at the SiC or defect sites. Total reduction in the Cl 2s intensity is also observed at the flash-annealing temperature of 1150 K (Figure 8f), suggesting possible Cl diffusion into the bulk and/or the carbon clusters.

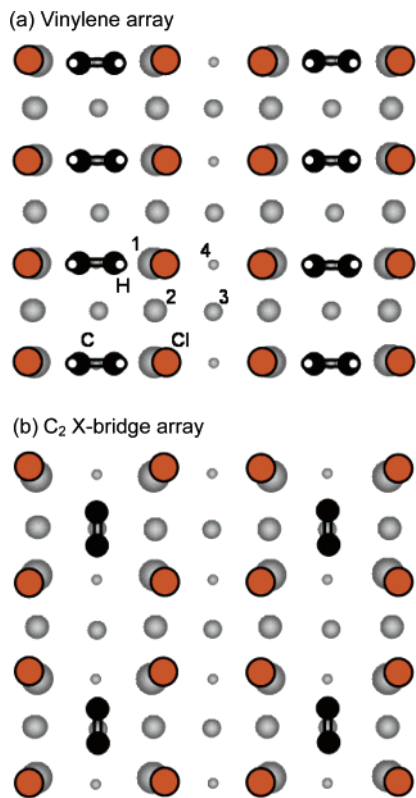


Figure 9. Schematic diagrams of ordered arrays of Cl atoms at the 1×1 sites with overlapping arrays of (a) vinylene and (b) C_2 dimer at the X-bridge site. Si atoms in the top (surface, layer 1) to bottom layers (layer 4) are represented by gray circles of decreasing diameters while the Cl, C, and H atoms are identified by open shaded circles, solid black circles, and open white circles.

4. Summary

Dissociative adsorption with insertion of Si atoms into C—Cl has been observed for both *cis*-DCE and PCE on $Si(100)2 \times 1$ in our XPS experiments. Unlike the cycloaddition mechanism found for ethylene, the C=C bonds in both chlorinated ethylenes remain intact in this insertion mechanism. The differences in the halogen content (and molecular structures) for these chlorinated ethylenes are found to lead to different novel chemisorption adstructures with different thermal evolution pathways. In particular, breakage of one and two C—Cl bonds in *cis*-DCE (via insertion of Si atoms) is found to produce mono- σ bonded 2-chlorovinyl and di- σ bonded vinylene adspecies, respectively (Figure 2). Similarly, C—Cl bond breakage in PCE could lead to mono- σ bonded trichlorovinyl and three plausible di- σ bonded adstructures, including dichlorovinylene in the cross-dimer bridge and in-plane dimer bridge sites, and dichlorovinylidene in the out-of-plane dimer bridge site (Figure 6). Furthermore, the remarkably large intensity ratio for the C_a 1s to C_c 1s XPS features provides strong evidence for total dechlorination and the formation of the novel tetra- σ bonded ethenetetrayl (or C_2 dimer) adspecies likely in an X-bridge geometry (Figure 6e).

TPD and temperature-dependent XPS experiments have also been conducted to investigate the thermally driven processes for the respective adstructures of *cis*-DCE and PCE on $Si(100)2 \times 1$. In particular, acetylene (m/z 26) is found to be the predominant desorption product (with desorption maxima at 590 and 750 K) for the adstructures of *cis*-DCE on the 2×1 surface. For *cis*-DCE, recombinative desorption of HCl (m/z 36) with desorption maximum at 850 K is found to be a prominent Cl removal channel. For PCE, Cl is removed primarily as an

etching product $SiCl_2$ (m/z 98) with desorption maximum at 870 K, while the formation of HCl is limited by the extent of the residual H atoms present on the surface. Evidently, the ready abundance of surface H atoms in the case of *cis*-DCE adsorption is sufficiently effective that the formation of $SiCl_2$ is not observed. Above 950 K, all the remaining adspecies for both *cis*-DCE and PCE are believed to have converted to SiC and/or (hydro)carbon clusters.

Although direct evidence for periodic arrangement of adstructures has not been obtained, the present work shows that both *cis*-DCE and PCE could be used to produce adstructures with local arrangements of C=C bonds and Cl atoms. Examples of two “ideal” templates using these adstructures as the building blocks are shown schematically in Figure 9. In particular, the rows of di- σ bonded vinylene adspecies for *cis*-DCE (Figures 9a and 2a) are potentially stabilized by adjacent rows of Cl atoms while the tetra- σ bonded C_2 dimers in the X-bridge sites for PCE (Figures 9b and 6e) are insulated by the four Cl corner atoms. These “hypothetical” arrays of alternating C=C bonds and neighboring Cl atoms could be useful for further silicon functionalization and molecular electronics applications.

Acknowledgment. This work was supported by the Natural Sciences and Engineering Research Council of Canada.

References and Notes

- Hamers, R. J.; Hovis, J. S.; Lee, S.; Liu, H.; Shan, J. J. *Phys. Chem. B* **1997**, *101*, 1489.
- Lin, Z.; Strother, T.; Cai, W.; Cao, X.; Smith, L. M.; Hamers, R. J. *Langmuir* **2002**, *18*, 788.
- Bozack, M. J.; Taylor, P. A.; Choyke, W. J.; Yates, J. T., Jr. *Surf. Sci.* **1986**, *177*, L933.
- Widdra, W.; Huang, C.; Yi, S. I.; Weinberg, W. H. *J. Chem. Phys.* **1996**, *105*, 5605.
- Rignanesse, G. M.; Blase, X.; Louie, S. G. *Phys. Rev. B* **2001**, *86*, 2110.
- Fisher, A. J.; Blöchl, P. E.; Briggs, G. A. D. *Surf. Sci.* **1997**, *374*, 298.
- Pan, W.; Zhou, T.; Yang, W. *J. Chem. Phys.* **1997**, *107*, 3981.
- Feng, K.; Liu, Z. H.; Lin, Z. *Surf. Sci.* **1995**, *329*, 77.
- Bronikowski, M. J.; Hamers, R. J. *J. Vac. Sci. Technol. A* **1995**, *13*, 777.
- Gutleben, H.; Lucas, S. R.; Cheng, C. C.; Choyke, W. J.; Yates, J. T., Jr. *Surf. Sci.* **1991**, *257*, 146.
- He, Z. H.; Yang, X.; Zhou, X. J.; Leung, K. T. *Surf. Sci.* **2003**, *547*, L840.
- Zhou, X. J.; Li, Q.; He, Z. H.; Yang, X.; Leung, K. T. *Surf. Sci.* **2003**, *543*, L668.
- Aldao, C. M.; Wearver, J. H. *Prog. Surf. Sci.* **2001**, *68*, 189.
- Okada, H.; Inagaki, K.; Goto, H.; Endo, K.; Hirose, K.; Mori, Y. *Surf. Sci.* **2002**, *515*, 287.
- Chen, D.; Boland, J. J. *Phys. Rev. B* **2003**, *67*, 195328.
- Li, Q.; Leung, K. T. *Surf. Sci.* **2001**, *479*, 69.
- Moulder, J. F.; Stickle, W. F.; Sobol, P. E.; Bomben, K. D. *Handbook of X-ray Photoelectron Spectroscopy*; Perkin-Elmer Corporation: Eden Prairie, MN, 1992.
- Fink, A.; Widdra, W.; Wurth, W.; Keller, C.; Stichler, M.; Achleitner, A.; Comelli, G.; Lizzit, S.; Baraldi, A.; Menzel, D. *Phys. Rev. B* **2001**, *64*, 045308.
- Frisch, M. J.; Trucks, G. W.; Schlegel, H. B.; Scuseria, G. E.; Robb, M. A.; Cheeseman, J. R.; Montgomery, J. A., Jr.; Vreven, T.; Kudin, K. N.; Burant, J. C.; Millam, J. M.; Iyengar, S. S.; Tomasi, J.; Barone, V.; Mennucci, B.; Cossi, M.; Scalmani, G.; Rega, N.; Petersson, G. A.; Nakatsuji, H.; Hada, M.; Ehara, M.; Toyota, K.; Fukuda, R.; Hasegawa, J.; Ishida, M.; Nakajima, T.; Honda, Y.; Kitao, O.; Nakai, H.; Klene, M.; Li, X.; Knox, J. E.; Hratchian, H. P.; Cross, J. B.; Adamo, C.; Jaramillo, J.; Gomperts, R.; Stratmann, R. E.; Yazyev, O.; Austin, A. J.; Cammi, R.; Pomelli, C.; Ochterski, J. W.; Ayala, P. Y.; Morokuma, K.; Voth, G. A.; Salvador, P.; Dannenberg, J. J.; Zakrzewski, V. G.; Dapprich, S.; Daniels, A. D.; Strain, M. C.; Farkas, O.; Malick, D. K.; Rabuck, A. D.; Raghavachari, K.; Foresman, J. B.; Ortiz, J. V.; Cui, Q.; Baboul, A. G.; Clifford, S.; Cioslowski, J.; Stefanov, B. B.; Liu, G.; Liashenko, A.; Piskorz, P.; Komaromi, I.; Martin, R. L.; Fox, D. J.; Keith, T.; Al-Laham, M. A.; Gonzalez, C. Y.; Pople, J. A. *Gaussian 03*, Revision A.1; Gaussian, Inc.: Pittsburgh, PA, 2003.

(20) Foresman, J. B.; Frisch, Æ. *Exploring Chemistry with Electronic Structure Methods*, 2nd ed.; Gaussian Inc.: Pittsburgh, PA, 1996; and references therein.

(21) Weast, R. C., Ed. *CRC Handbook of Chemistry and Physics*, 64th ed.; CRC Press: Baton Raton, FL, 1983.

(22) Flowers, M. C.; Jonathan, N. B. H.; Liu, Y.; Morris, A. *J. Phys. Chem.* **1993**, *99*, 7038.

(23) Siegbahn, K.; Nordling, C.; Johansson, G.; Hedman, J.; Heden, P.-F.; Hamrin, K.; Gelius, U.; Bergmark, T.; Werne, L. O.; Manne, R.; Baer, Y. *ESCA Applied to Free Molecules*; North-Holland: New York, 1969.

(24) Briggs, D.; Seah, M. P. *Practical Surface Analysis by Auger and X-ray Photoelectron Spectroscopy*; Wiley: New York, 1983.

(25) Brown, K. A.; Ho, W. *Surf. Sci.* **1995**, *338*, 111.

(26) Pauling, L. *The Nature of the Chemical Bond*; Cornell University Press: Ithaca, NY, 1960.

(27) Park, K. T.; Klier, K.; Wang, C. B.; Zhang, W. X. *J. Phys. Chem. B* **1997**, *101*, 5420.

(28) Cassuto, A.; Hugenschmidt, M. B.; Parent, P.; Laffon, C.; Tourillon, H. G. *Surf. Sci.* **1994**, *310*, 390.

(29) Coulter, S. K.; Schwartz, M. P.; Hamers, R. J. *J. Phys. Chem. B* **2001**, *105*, 3079.

(30) Smentkowski, V. S.; Cheng, C. C.; Yates, J. T. *Surf. Sci.* **1989**, *220*, 307.

(31) Nakayama, K.; Graugnard, E.; Weaver, J. H. *Phys. Rev. Lett.* **2002**, *88*, 125508.

(32) Koleske, D. D.; Gates, S. M. *J. Chem. Phys.* **1993**, *98*, 5091.